JOURNAL OF GUIDANCE, CONTROL, AND DYNAMICS
Vol. 19, No. 4, July–August 1996

Adaptive Control of a Zero-Stiffness Suspension System

Li-Farn Yang,* Rueih-Chir Tzeng,† and Chun-Pao Kuo‡
National Chung Cheng University, Chia-Yi 621, Taiwan, Republic of China

A zero-stiffness suspension system featuring a noncircular disk is used as an application in counteracting gravity loads in ground-based structural testing. The dynamic behavior of this mechanism is analyzed in closed form, in which this mechanism is shown to be very sensitive to inertial properties of a noncircular disk, which can introduce inertial forces to trigger nonlinear dynamic behavior in the system, thereby degrading testing performance under such inertial loading. An adaptive feedforward control law is developed for eliminating these inertial effects on the suspension system during dynamic testing. Under this control manipulation, the output signals of disk mechanism are regulated and tracked along the desired trajectories so that the error signals can be vastly reduced. Stability of the control system is investigated, and simulated time histories of test articles under an active band-drive suspension system also are presented to show the effectiveness of the approach.

Nomenclature

$\boldsymbol{A}$	= null-space matrix of Jacobian matrix $\boldsymbol{B}$
$\boldsymbol{B}$	= constraint Jacobian matrix
$\boldsymbol{C}$	= damping matrix of equations of motion
c_v	= viscous drag coefficient of motor
e_a	= applied voltage of armature
e_f	= applied voltage of armature from adaptation law
$\boldsymbol{F}$	= forcing vector of equations of motion
$G(s)$	= transfer function in s-domain
g_s, g_v	= constant feedback gains
I_c	= moment-of-inertia of noncircular disk
I_m	= moment-of-inertia of armature
$\boldsymbol{K}$	= stiffness matrix of equations of motion
k_b	= back-emf constant of motor
k_j	= spring stiffness of the jth spring
k_s	= torsional spring stiffness
k_t	= torque constant of motor
ℓ_j	= static elongation of the jth spring
$\boldsymbol{M}$	= mass matrix of equations of motion
m_i	= mass of the ith body
N_g	= gear ratio
R_a	= armature resistance of motor
r_a	= distance between disk center and ring
r_b	= pitch radius of noncircular disk
W	= total weight of test articles
$\boldsymbol{y}$	= vector of state variables, $[y_1, \ldots, y_n]^T$
y_i	= displacement of the ith body
γ	= adaptation gain
ϵ	= sum of error signals, $\varepsilon(t) + \dot{\varepsilon}(t)$
$\varepsilon(t)$	= error signal, $\theta_d(t) - \theta(t)$
θ	= angular displacement of noncircular disk
$\theta_d(t)$	= desired trajectory of disk angle
θ_m	= angular displacement of motor
$\boldsymbol{\lambda}$	= vector of Lagrangian multipliers
$\boldsymbol{\xi}$	= vector of state variables, $[\theta, y_1, \ldots, y_n]^T$
τ_a	= available torque from motor shaft
τ_s	= actuating torque from motor to disk shaft
$\boldsymbol{\Phi}$	= nonholonomic constraint equations
ϕ	= angular displacement of cable
$\varphi(t)$	= vector of adaptation variables
ω_s, ω_v, ω_a	= adaptation variables

Received July 13, 1995; revision received Jan. 5, 1996; accepted for publication Feb. 18, 1996.

*Associate Professor, Department of Mechanical Engineering. Member AIAA.
†Research Assistant, Department of Mechanical Engineering.
‡Associate Professor, Department of Mechanical Engineering.

I. Introduction

FLEXIBLE space structures, in general, experience free–free boundary conditions that are not readily replicable on Earth. Yet, to test these space structures, special suspension devices are needed to support the weight of the structure without introducing any constraint forces, which in turn impose additional boundary conditions that do not simulate the desired free–free boundary conditions in space. Various concepts and approaches have been proposed for counteracting gravity loads on space structures for ground-based dynamic testing.[1–4] Chew et al.[1] has surveyed several existing suspension devices including long cables, air pads, pneumatic/electric devices,[2] soft springs, zero-spring-rate systems,[3] and band-drive suspension systems.[4] Their study indicated that a band-drive suspension system has many advantages over other candidates, such as compact size, low friction, absence of air tank and mechanical maintenance, and wide-range working domain for zero-stiffness rate. Also, the band-drive suspension system is capable of keeping the test structures in static equilibrium at any given vertical position and of simulating the constant-speed motion for test structures in response to an impulse.

A band-drive suspension system, such as that shown in Fig. 1, offers a zero-gravity suspension environment needed on ground for dynamic testing of space structures. The system consists of a noncircular disk over which a wraparound cable winds and unwinds as the disk rotates. This disk has a special profile that is developed from the kinematic perspective that the inertial properties of the disk are neglected in the design procedure. However, in practice, the inertial properties exist with the disk and give rise to the inertial forces loaded on the suspension system, which can initiate nonlinear behavior on the disk dynamics. The effects of inertial loads upon the

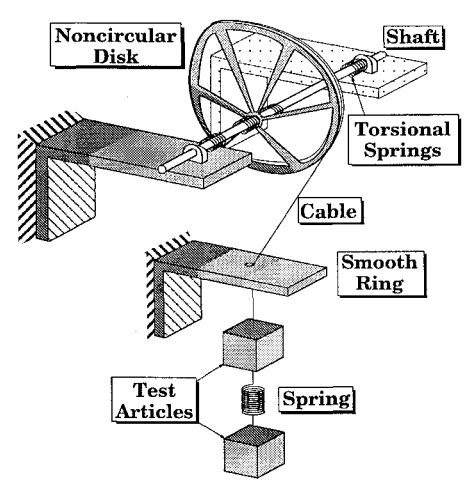

Fig. 1 Configuration of a band-drive suspension system.

band-drive suspension system are all adverse and result in malfunction of countergravitational operations or even in instability of the system. The undesirable inertial loads can be eliminated by means of active control; however, some issues must be considered in advance, for instance: 1) dynamics loaded by the disk inertia may vary with different operating conditions, 2) inertial loads of the disk have to be actively counteracted during transient as well as at steady state, and 3) control design must remain unchanged for test articles with different weights, wherein conventional feedback control does not seem entirely effective and satisfactory for such purposes. The objective of this paper is to eliminate the time-varying inertial loading inherent in the band-drive suspension system from the standpoint of adaptive control. In particular, an adaptive trajectory tracking under a model reference adaptive feedforward control is considered.

This paper uses an adaptive feedforward control scheme[5] intended to adjust the inertial loads for an active band-drive suspension system in conducting the structural testing. Included in the closed-loop system is a model reference adaptive controller composed of a fixed-gain feedback control and an adaptive feedforward control. Early applications of this control concept were restricted to self-tuning regulators, but new applications are emerging, e.g., motion synchronization of x-y tables in contouring,[6] of twin-gyro control moment gyroscopes in precessing,[7] and of magnetic bearings in levitating.[8] It is known[5] that the adaptive feedforward control is very effective in tracking and error regulation when there exists a measurably uncertain payload acting on the systems, which makes the present method well suited to the suspension control problem relative to the inertial loading. The closed-loop performance under the adaptive feedforward control closely matches that of a reference model that characterizes a rule of motion governing the disk kinematics in the absence of inertial loading. Stability analysis of the overall control system is also conducted in a determining a stable margin for an adaptation gain in the sense of asymptotic stability.

The remainder of this paper is organized as follows: First, the description of system dynamics is presented for the band-drive suspension system incorporating a controlled dc motor. Second, the nonlinear dynamic behavior of the band-drive suspension system related to inertial loading effects is analyzed with a closed-form solution. Then, the derivation of an adaptive feedforward controller is detailed and applied to the band-drive suspension system. Finally, the simulation results of transient responses, subjected to the excitations of initial displacement and initial velocity, are presented for discussion.

II. System Dynamics

In this section, dynamics of a disk mechanism and an actuator are studied and incorporated into an active band-drive suspension system, as shown in Fig. 2. This paper considers the utilization of a dc motor as an actuating device. A multibody dynamic model is formulated for this motor-equipped suspension system with lumped test articles for the dynamics and control analysis. In what follows, we begin with the derivation of equations of motion for this suspension system with motor and test articles onboard.

A. Multibody Dynamics of a Band-Drive Suspension System

A band-drive suspension system with test articles can be modeled as a multibody dynamic system in which a noncircular disk is preloaded by the torsional springs at its center of rotation and pulled by a cable connected to n serial lumped articles underneath the disk mechanism. As shown in Fig. 2, the disk has a convex profile that allows a wraparound cable to overlap it and extend downward to suspend the test objects. The disk profile is designed using envelope theory,[4] and the test articles can be characterized by n masses and $(n-1)$ connecting springs as a lumped-parameter system.

Wherever the system is at rest, the static equilibrium of the forces must satisfy the following equations[4]:

$$W = \frac{k_s\theta_o}{r_a \sin\phi_o} = \frac{k_s(\theta+\theta_o)}{r_a \sin(\phi+\phi_o)} \tag{1}$$

$$k_j \ell_j = \sum_{i=j}^{n} m_i g \qquad \text{for} \qquad j = 2, \ldots, n \tag{2}$$

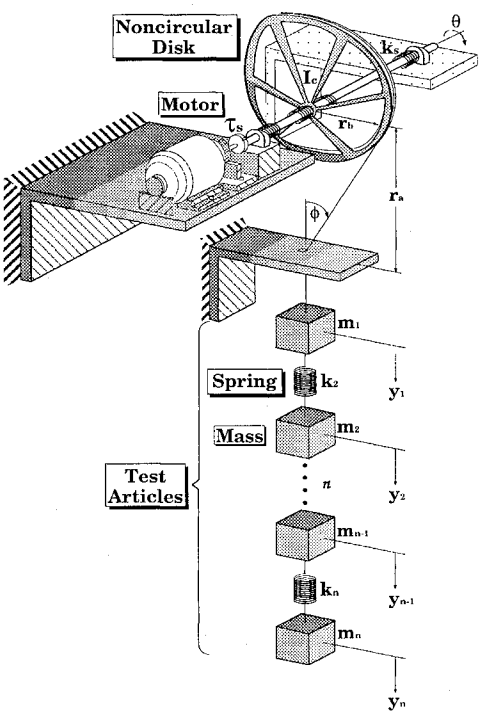

Fig. 2 Motor-equipped suspension system with multiple test articles.

where $W = \sum_{i=1}^{n} m_i g$, $\phi_o = \sin^{-1}(r_b/r_a)$, and $\theta_o = (W/k_s)r_b$. Because θ varies according to Eq. (1), it is possible for the test articles to remain in static equilibrium when displaced from one position of static equilibrium to another, so that a weightless effect can be simulated on Earth through this suspension system. Note that the displacement y_1 of mass m_1 must be consistent with the disk angle θ because the suspension cable is directly connected to mass m_1. The displacement y_1 can be equated by integrating along the curvilinear path of the disk profile through the rotation θ so that

$$y_1 = \int_0^{\theta} r_a \sin(\phi+\phi_o)\,\mathrm{d}\theta = \frac{k_s}{W}\left(\frac{\theta^2}{2} + \theta_o\theta\right) \tag{3}$$

If the displacement y_1 is given, the above quadratic function can be solved by

$$\theta + \theta_o = (W/k_s)\sqrt{r_b^2 + 2(k_s/W)y_1} \tag{4}$$

Differentiating Eqs. (3) and (4) with respect to time yields

$$\dot{y}_1 = \frac{k_s}{W}(\theta+\theta_o)\dot{\theta} \qquad \text{and} \qquad \dot{\theta} = \frac{\dot{y}_1}{\sqrt{r_b^2 + 2(k_s/W)y_1}} \tag{5}$$

which is, in fact, a velocity constraint between $\dot{y}_1$ and $\dot{\theta}$.

Applying d'Alembert's principle of virtual work,[9] the equations of motion of the band-drive suspension system in conjunction with the test articles can be expressed in the following matrix form:

$$\boldsymbol{M}\ddot{\xi} + \boldsymbol{K}\xi + \boldsymbol{B}^T\lambda = \boldsymbol{F} \qquad \text{and} \qquad \boldsymbol{\Phi} = \boldsymbol{B}\dot{\xi} = 0 \tag{6}$$

To be more detailed, the mass matrix, the forcing vector, and the stiffness matrix can be written as

$$\boldsymbol{M} = \mathrm{Diag}[I_c, m_1, \ldots, m_n]$$

$$\boldsymbol{F} = [f_s, f_1, \ldots, f_n]^T \tag{7}$$

$$\boldsymbol{K} = \begin{bmatrix} k_s & 0 & 0 & 0 & \cdots & \cdots & \cdots & 0 \\ 0 & k_2 & -k_2 & 0 & \cdots & \cdots & \cdots & \vdots \\ 0 & -k_2 & k_2+k_3 & -k_3 & \cdots & \cdots & \cdots & \vdots \\ & & & & \ddots & & & \\ 0 & \cdots & \cdots & \cdots & \cdots & -k_{n-1} & k_{n-1}+k_n & -k_n \\ 0 & \cdots & \cdots & \cdots & \cdots & 0 & -k_n & k_n \end{bmatrix}$$

where

$$\begin{aligned} f_s &= \tau_s - k_s\theta_o \\ f_1 &= m_1 g + k_2 l_2 \\ f_i &= m_i g - k_i l_i + k_{i+1} l_{i+1} \qquad \text{for} \qquad i = 2, \ldots, n-1 \\ f_n &= m_n g - k_n l_n \end{aligned} \tag{8}$$

The Jacobian matrix $\boldsymbol{B}$ configuring the kinematic constraints for this band-drive suspension system is derived by including the velocity constraint equation (5), which can be arranged as

$$\boldsymbol{B} = \begin{bmatrix} 1 & -\dfrac{1}{\sqrt{r_b^2 + 2(k_s/W)y_1}} & 0 & \cdots & 0 \\ 0 & 0 & 0 & \cdots & 0 \\ \vdots & \vdots & \vdots & \ddots & \vdots \\ 0 & 0 & 0 & \cdots & 0 \end{bmatrix}_{(n \times n+1)} \tag{9}$$

The Jacobian matrix as given by Eq. (9) can be removed from Eq. (6) through a null-space elimination process,[9] such that

$$\dot{\xi} = \boldsymbol{A}\dot{\boldsymbol{y}} \qquad \text{and} \qquad \boldsymbol{y} = [y_1, \ldots, y_n]^T \tag{10}$$

where

$$\boldsymbol{A} = \begin{bmatrix} \dfrac{1}{\sqrt{r_b^2 + 2(k_s/W)y_1}} & 0 & \cdots & \cdots & 0 \\ 1 & 0 & \cdots & \cdots & 0 \\ 0 & 1 & 0 & \cdots & \vdots \\ \vdots & 0 & 1 & & \vdots \\ \vdots & \vdots & & \ddots & 0 \\ 0 & \cdots & \cdots & 0 & 1 \end{bmatrix}_{(n+1 \times n)} \tag{11}$$

The transformation matrix $\boldsymbol{A}$ in Eq. (11) is a complement of the Jacobian matrix $\boldsymbol{B}$ so that the orthogonal relation, $\boldsymbol{BA} = 0$, holds. Premultiplying Eq. (6) with the transpose of matrix $\boldsymbol{A}$ and substituting $\ddot{\xi}$ with $\dot{\boldsymbol{y}}$ and $\dot{\boldsymbol{y}}$ derived from Eq. (10), one can obtain

$$\boldsymbol{A}^T\boldsymbol{M}\boldsymbol{A}\ddot{\boldsymbol{y}} + \boldsymbol{A}^T\boldsymbol{M}\dot{\boldsymbol{A}}\dot{\boldsymbol{y}} + \boldsymbol{A}^T\boldsymbol{K}\hat{\boldsymbol{A}}\boldsymbol{y} = \boldsymbol{A}^T\boldsymbol{F} \tag{12}$$

where

$$\dot{\boldsymbol{A}} = \begin{bmatrix} -\dfrac{(k_s/W)}{\sqrt{\left[r_b^2 + 2(k_s/W)y_1\right]^3}} & 0 & \cdots & \cdots & 0 \\ 0 & 0 & \cdots & \cdots & 0 \\ 0 & 0 & 0 & \cdots & \vdots \\ \vdots & 0 & 0 & & \vdots \\ \vdots & \vdots & & \ddots & 0 \\ 0 & \cdots & \cdots & 0 & 0 \end{bmatrix}$$

and

$$\hat{\boldsymbol{A}} = \begin{bmatrix} \dfrac{(W/k_s)}{2\sqrt{r_b^2 + 2(k_s/W)y_1}} & 0 & \cdots & \cdots & 0 \\ 1 & 0 & \cdots & \cdots & 0 \\ 0 & 1 & 0 & \cdots & \vdots \\ \vdots & 0 & 1 & & \vdots \\ \vdots & \vdots & & \ddots & 0 \\ 0 & \cdots & \cdots & 0 & 1 \end{bmatrix} \tag{13}$$

The angular displacement and velocity of the disk may be determined from Eqs. (4) and (5) during the simulation process, even though they do not appear explicitly in Eq. (12).

Equation (12) thus provides a set of λ-free differential equations capable of implementing the open-loop simulations of a band-drive suspension system subject to any excitations. In the following section, we model a dc motor and attempt to integrate both actuator and suspension system dynamics as a whole in closed loop for control analysis.

B. Actuator Dynamics

The actuator shown in Fig. 2 is directly connected to the shaft of the noncircular disk. A step-down gear box can be built into the actuator to proportionally magnify the output torque if needed. The dc motor can be modeled by a standard armature circuit, which is governed by the following differential equation:

$$I_m\ddot{\theta}_m + [c_v + (k_t k_b/R_a)]\dot{\theta}_m + \tau_a = (k_t/R_a)e_a \tag{14}$$

The τ_a and θ_m in Eq. (14) are then transformed to τ_s and θ, respectively, through a step-down constant gear ratio N_g, so that

$$\tau_a = N_g\tau_s \qquad \text{and} \qquad \theta_m = (1/N_g)\theta \tag{15}$$

Substituting Eq. (15) into Eq. (14), the output torque τ_s to the disk is obtained and can be expressed by

$$\tau_s = \frac{k_t}{R_a N_g}e_a - \frac{c_v + (k_t k_b/R_a)}{N_g^2}\dot{\theta} + \frac{I_m}{N_g^2}\ddot{\theta} \tag{16}$$

The input voltage e_a across the actuator in Eq. (16) will be generated according to the adaptive feedforward controller in actuating the noncircular disk. Substituting Eq. (16) into Eq. (6), we obtain an electromechanical model for the active band-drive suspension system, which can be presented as

$$\bar{\boldsymbol{M}}\ddot{\xi} + \boldsymbol{C}\dot{\xi} + \boldsymbol{K}\xi + \boldsymbol{B}^T\lambda = \bar{\boldsymbol{F}} \tag{17}$$

where

$$\begin{aligned} \bar{\boldsymbol{M}} &= \mathrm{Diag}\left[I_c + \left(I_m/N_g^2\right), m_1, \ldots, m_n\right] \\ \boldsymbol{C} &= \mathrm{Diag}\left[\frac{c_v + (k_t k_b/R_a)}{N_g^2}, 0, \ldots, 0\right] \\ \bar{\boldsymbol{F}} &= [f_s', f_1, \ldots, f_n]^T, \qquad f_s' = (k_t/R_a N_g)e_a + k_s(\theta + \theta_o) \end{aligned} \tag{18}$$

Premultiplying Eq. (17) with the transpose of matrix $\boldsymbol{A}$ and substituting $\ddot{\xi}$ with $\dot{\boldsymbol{y}}$ and $\ddot{\boldsymbol{y}}$ derived from Eq. (10) yield

$$\boldsymbol{A}^T\bar{\boldsymbol{M}}\boldsymbol{A}\ddot{\boldsymbol{y}} + (\boldsymbol{A}^T\bar{\boldsymbol{M}}\dot{\boldsymbol{A}} + \boldsymbol{A}^T\boldsymbol{C}\boldsymbol{A})\dot{\boldsymbol{y}} + \boldsymbol{A}^T\boldsymbol{K}\hat{\boldsymbol{A}}\boldsymbol{y} = \boldsymbol{A}^T\bar{\boldsymbol{F}} \tag{19}$$

which can implement the closed-loop simulations of the band-drive suspension system in conjunction with an actively controlled actuator.

As can be seen in Eq. (18), the inertial loads of the disk mechanism reside in the mass matrix, including the moments of inertia of the disk and the motor; the latter is usually small and negligible compared to the former. These inertial loads are the leading factors resulting in the dynamic nonlinearities in the suspension system, which are studied in the Sec. III.

III. Analysis of Inertial Loading Effects

The simplest model for analyzing the dynamic behavior of the band-drive suspension system affected by its inertial loads is to suspend a single mass via a cable without considering control efforts. This facilitates the study of the impulsive responses of a suspended mass excited by an impulse. Ideally, such single mass should undergo a constant-speed motion as a free body would react in space. A governing equation of motion for the single-mass suspension dynamics can be derived from Eq. (19) with the actuator removed, which becomes

$$\left[I_c + m_1(k_s/W)^2(\theta + \theta_o)^2\right]\ddot{\theta} + m_1(k_s/W)^2(\theta + \theta_o)\dot{\theta}^2 = 0 \tag{20}$$

It can be deduced that Eq. (20) can be exactly integrated in time, and the closed-form solution can be expressed by

$$t = \frac{1}{2}(\theta+\theta_o)\sqrt{I_c + m_1\left(\frac{k_s}{W}\right)^2(\theta+\theta_o)^2} + \frac{1}{2}\frac{I_c W}{k_s\sqrt{m_1}} \times \ell_n\left[\sqrt{m_1}\frac{k_s}{W}(\theta+\theta_o) + \sqrt{I_c + m_1\left(\frac{k_s}{W}\right)^2(\theta+\theta_o)^2}\right] \quad (21)$$

which presents a highly nonlinear relationship between the time t and the disk angle θ. The closed-form solution shown in Eq. (21) does not satisfy the kinematic relations given by Eqs. (4) and (5) because of the existence of the disk inertia loads. This can be interpreted by assuming that the moment of inertia of the disk, I_c, is negligible in Eq. (20), so that one can end up with a simple kinematic relationship:

$$\ddot{\theta} = -[1/(\theta+\theta_o)]\dot{\theta}^2 \Longrightarrow \ddot{\theta}/\dot{\theta} = -[\dot{\theta}/(\theta+\theta_o)] \quad (22)$$

which is consistent with Eqs. (4) and (5) for the dynamic description of a suspended mass traveling at a constant velocity during the impulsive responses. This also implies an important rule that the ratio of angular acceleration to angular velocity is equivalent to the negative ratio of angular velocity to angular position of the disk in the absence of inertial loading, which provides a good candidate as a reference model for the adaptive-control design developed in Sec. IV. Moreover, the solution to Eq. (22) yields

$$t = \frac{1}{2}\frac{\sqrt{m_1}k_s}{W}(\theta+\theta_o)^2$$

which is obtained from Eq. (21) by letting $I_c = 0$.

The inertial effects on the disk dynamics can be perceived by studying the sensitivity of the disk angle vs the moment of inertia of the disk. The sensitivity equation is derived by 1) partial differentiation of the closed-form function, as shown in Eq. (21), with respect to θ and I_c and 2) using the chain rule to obtain the sensitivity equation of $(\partial\theta/\partial I_c)$ in closed form, which is governed by

$$\frac{\partial\theta}{\partial I_c} = \frac{p + \dfrac{m_1}{p}\left(\dfrac{k_s}{W}\right)^2(\theta+\theta_o)^2 + \dfrac{I_c\left[\sqrt{m_1}(k_s/W) + (m_1/p)(k_s/W)^2(\theta+\theta_o)^2\right]}{\sqrt{m_1}(W/k_s)[\sqrt{m_1}(k_s/W)(\theta+\theta_o)+p]}}{\dfrac{1}{p}(\theta+\theta_o) + \dfrac{1}{\sqrt{m_1}}\dfrac{W}{k_s}\ell_n\left[\sqrt{m_1}\dfrac{k_s}{W}(\theta+\theta_o)+p\right] + \dfrac{I_c W}{2\sqrt{m_1}k_s}\dfrac{1}{[\sqrt{m_1}(k_s/W)(\theta+\theta_o)+p]}} \quad (23)$$

where $p = \sqrt{[I_c + m_1(k_s/W)^2(\theta+\theta_o)^2]}$. To compute the value of the sensitivity in Eq. (23), one needs to solve the closed-form function given by Eq. (21) to achieve the value of the disk angle θ for any given time t. Figure 3 illustrates this sensitivity result for different values of disk angles and moments of inertia by evaluating Eq. (23) with parameters listed in Table 1. The magnitude of sensitivity increases with the increments of inertial loads and saturates around 0.36 for any given disk angle. Hence, the disk dynamics are very sensitive to the inertial loading embedded in the disk mechanism, which causes the nonlinear behavior in the dynamic responses and poses a severe restriction on the band-drive suspension system for the structural testing.

Here, we use a single-mass suspension model for analysis, but when multiple masses are considered, the large motion could potentially degrade suspension performance in the presence of inertial loading. To counterbalance those inertial loads, we attempt to design a control system in terms of an adaptive feedforward control scheme for an active band-drive suspension system. This is investigated in Sec. IV.

Table 1 Model parameters of a band-drive suspension system

Parameters	Units	Parameters	Units
Disk mechanism			
$r_a = 12.0$	in.	$r_b = 6.0$	in.
$\phi_o = 30.0$	deg	$I_c = 10.0$	lb-in.^{2}
$k_s = 0.5$	in.-lb/rad	—	—
DC motor			
$I_m = 4.7 \times 10^{-5}$	lb-in.^{2}	$k_t = 3.46 \times 10^{-2}$	N · m/A
$k_b = 3.42 \times 10^{-2}$	N · m/A	$R_a = 4.0$	Ω
$c_v = 1.0 \times 10^{-4}$	V · rad^{-1} s^{-1}	$N_g = 1.0$	—
Test articles			
$m_1 = 12.0$	lb	$m_2 = 12.0$	lb
$k_2 = 1.0$	lb/rad	—	—
Adaptive feedforward control law			
$\gamma = 80$	$g_s = 120$	—	—
$g_v = 60$	—	—	—

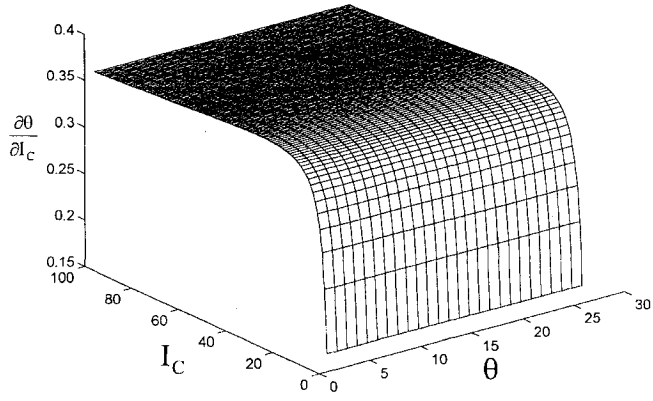

Fig. 3 Sensitivity of disk angle vs moment of inertia of disk.

IV. Control System

As alluded to in the preceding section, the band-drive suspension system must be capable of handling the test articles with different weights and be robust to the substantial nonlinearities in the system characteristics introduced by the disk inertia loads; therefore, model reference adaptive schemes seem particularly well suited for such control purposes. We make concurrent use of adaptive control and feedforward control, and assess their applicability to the active control of the band-drive suspension system. An adaptive feedforward controller thus is integrated, with the merits of each particular control included. First, the feedforward control is known to be very effective in tracking the time-varying desired output signal as long as the nonlinear character is measurable and the plant model is accurate. Then, when system parameters slowly vary, adding adaptation into the feedforward control can enable the resulting system to deal with the varying plant parameters and eliminate the steady-state error caused by the feedforward control. In so doing, the time-varying output signals measured from the disk mechanism are regulated and tracked along the desired trajectories so that the tracking errors resulting from inertial loading of system are greatly reduced.

A. Adaptive Feedforward Control

The development of the compensation network and parameter adjustment mechanism follows the adaptive feedforward control

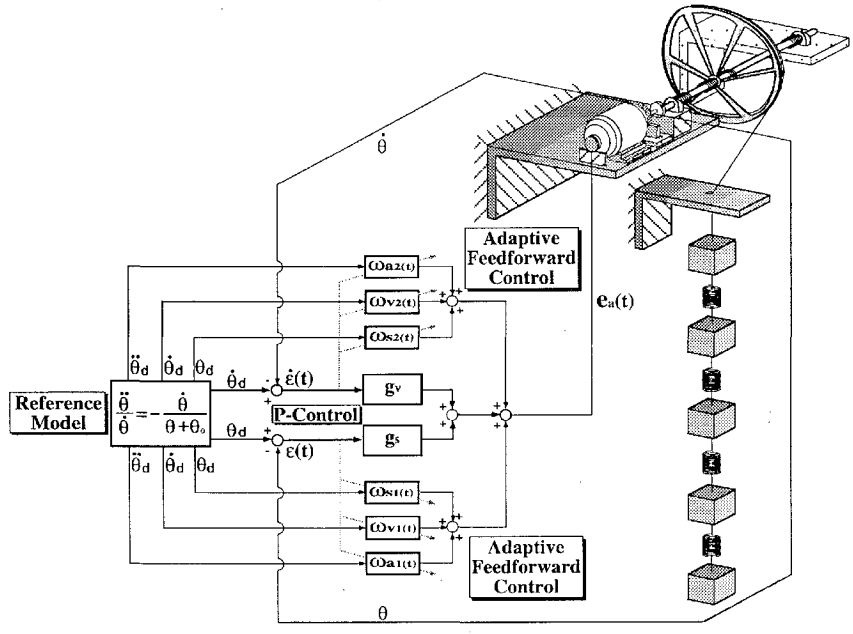

Fig. 4 Adaptive feedforward control block diagram.

algorithm. Figure 4 shows a control block diagram of the proposed control system. As demonstrated in Fig. 4, the adaptive feedforward control is attributed to the model reference type, which requires a reference model against which system performance is measured. The reference model is a relatively simple model of the disk, which must obey the rule of motion as specified in Eq. (22), and can properly be driven by the inputs to provide the time-history trajectories of the disk angle θ_d and the angular velocity $\dot{\theta}_d$ as the desired signals. Then, corresponding to the transient responses, the error $\varepsilon(t)$ and the rate of error $\dot{\varepsilon}(t)$ can be obtained by defining $\varepsilon(t) = \theta_d(t) - \theta(t)$ and $\dot{\varepsilon}(t) = \dot{\theta}_d(t) - \dot{\theta}(t)$, respectively. These error signals are regulated through the feedback controller characterized by a fixed-gain control law incorporating a pair of variant adaptation laws in compensating for the tracking errors of $\varepsilon(t)$ and $\dot{\varepsilon}(t)$, respectively. A complete derivation of this control synthesis follows.

To introduce the adaptive feedforward control to the band-drive suspension system through an onboard dc motor, we start with the control input for the motor. As shown in Fig. 4, the input to the motor, i.e., e_a as defined in Eq. (14), can be obtained by

$$e_a(t) = [g_s \quad g_v]\begin{bmatrix}\varepsilon(t)\\ \dot{\varepsilon}(t)\end{bmatrix} + e_f(t) \tag{24}$$

where the error $\varepsilon(t)$ varies as a result of the difference between $\theta_d(t)$ and $\theta(t)$ when the noncircular disk is dynamically affected by its own inertia, and thereby deviating from the desired trajectory. Equation (24) can be interpreted as the combination of a regulator and an adaptive controller, in which the former as a vector product of fixed gains and errors cooperates with the latter, which can be adjusted by an adaptation law such as

$$e_f(t) = [\omega_{s1}(t) + \omega_{s2}(t)]\theta_d(t) + [\omega_{v1}(t) + \omega_{v1}(t)]\dot{\theta}_d(t) + [\omega_{a1}(t) + \omega_{a2}(t)]\ddot{\theta}_d(t) \tag{25}$$

where the adjustable parameters $\omega_{si}(t)$, $\omega_{vi}(t)$, and $\omega_{ai}(t)$ are adjusted for the adaptation input $e_f(t)$ through a set of first-order differential equations governed by

$$\begin{aligned}
\dot{\omega}_{s1}(t) &= \gamma\theta_d(t)\varepsilon(t), & \dot{\omega}_{s2}(t) &= \gamma\theta_d(t)\dot{\varepsilon}(t)\\
\dot{\omega}_{v1}(t) &= \gamma\dot{\theta}_d(t)\varepsilon(t), & \dot{\omega}_{v2}(t) &= \gamma\dot{\theta}_d(t)\dot{\varepsilon}(t)\\
\dot{\omega}_{a1}(t) &= \gamma\ddot{\theta}_d(t)\varepsilon(t), & \dot{\omega}_{a2}(t) &= \gamma\ddot{\theta}_d(t)\dot{\varepsilon}(t)
\end{aligned} \tag{26}$$

where γ is a positive adaptation gain that is selected from stability considerations to obtain the well-behaved and stable responses in the adjusting mechanism. According to the Massachusetts Institute of Technology (MIT) rule,[5] the adjustable parameters $\omega_{si}(t)$, $\omega_{vi}(t)$, and $\omega_{ai}(t)$ are fine-tuned in the manner shown in Eq. (26) to minimize a loss function specified by $J = \frac{1}{2}(\varepsilon^2 + \dot{\varepsilon}^2 + \ddot{\varepsilon}^2)$, whereas those adaptation parameters are instantaneously changed in the direction opposite to the gradient of the loss function. Based on the MIT rule for adaptive feedforward control, the sensitivities of the error signals with respect to the corresponding adaptation parameters are given by

$$\frac{\partial\varepsilon}{\partial\omega_{si}} = -\theta_d, \qquad \frac{\partial\dot{\varepsilon}}{\partial\omega_{vi}} = -\dot{\theta}_d, \qquad \frac{\partial\ddot{\varepsilon}}{\partial\omega_{ai}} = -\ddot{\theta}_d$$

which contribute to the formulation of the right-hand side of Eq. (26). The adaptation law in Eq. (26) can be rewritten as

$$\dot{\varphi}(t) = \gamma\varpi(t)\epsilon(t) \tag{27}$$

where

$$\varphi(t) = [\omega_{s1}(t) + \omega_{s2}(t) \quad \omega_{v1}(t) + \omega_{v2}(t) \quad \omega_{a1}(t) + \omega_{a2}(t)]^T$$

$$\varpi(t) = [\theta_d(t) \quad \dot{\theta}_d(t) \quad \ddot{\theta}_d(t)]^T$$

$$\epsilon(t) = \varepsilon(t) + \dot{\varepsilon}(t)$$

for the sake of stability analysis conducted later. Note that, in Eq. (27), $\omega_{si}(t)$ is driven by the position-error signal $\varepsilon(t)$ in the first-order differential equation, $\omega_{vi}(t)$ by the rate-error signal $\dot{\varepsilon}(t)$, and $\omega_{ai}(t)$ by the acceleration-error signal $\ddot{\varepsilon}(t)$.

To mechanize this control algorithm, one must solve the differential equation (22) given the initial condition to obtain the values of $\theta_d(t)$, $\dot{\theta}_d(t)$, and $\ddot{\theta}_d(t)$. These values are then multiplied with the corresponding error signals, and the resulting products are used as the forcing functions for Eq. (27). These first-order differential equations yield the values for $\omega_{si}(t)$, $\omega_{vi}(t)$, and $\omega_{ai}(t)$ as necessary in Eq. (25) to achieve the adaptation input $e_f(t)$.

B. Stability Analysis

The stability of the proposed adaptive system is investigated using the linearized model of the suspension system derived from Eq. (19). Combining this equation with the reference model described by Eq. (22) and with the adaptive feedforward mechanism represented by Eq. (27) results in the following state-variable equation:

$$\ddot{\theta}(t) + a\dot{\theta}(t) + b\theta(t) = c[g_s\varepsilon(t) + g_v\dot{\varepsilon}(t) + e_f(t)] \tag{28}$$

where a, b, and c are the lumped parameters depending on the inertial loads, the stiffness, and the viscous friction of the original

system. Substituting $\theta_d(t)-\varepsilon(t)$ for $\theta(t)$ in Eq. (28), one can present adaptation error dynamics described by

$$(1/c)[\ddot{\varepsilon}(t)+(a+cg_v)\dot{\varepsilon}(t)+(b+cg_s)\varepsilon(t)]$$
$$=[(1/c)-\omega_{a1}(t)-\omega_{a2}(t)]\ddot{\theta}_d+[(a/c)-\omega_{v1}(t)-\omega_{v2}(t)]\dot{\theta}_d$$
$$+[(b/c)-\omega_{s1}(t)-\omega_{s2}(t)]\theta_d \tag{29}$$

The left-hand side of Eq. (29) represents the plant of the error dynamics with the fixed proportional gain, whereas the right-hand side is the adaptation control for the desired output. Now, we define

$$G(s)=\frac{c}{s^2+(a+cg_v)s+(b+cg_s)} \quad \text{and} \quad \hat{\varphi}=\frac{1}{c}[b\ \ a\ \ 1]^T \tag{30}$$

Taking the Laplacian transform of Eq. (28) yields

$$\boldsymbol{L}\{\varepsilon(t)\}=-G(s)\boldsymbol{L}\{\tilde{\varphi}^T(t)\varpi(t)\} \tag{31}$$

where $\tilde{\varphi}(t)=\varphi(t)-\hat{\varphi}$. $G(s)$ in the feedforward path of this feedback system is positively definite and $\varpi(t)$ is well bounded because its elements $\theta_d(t)$, $\dot{\theta}_d(t)$, and $\ddot{\theta}_d(t)$ are all bounded, and so the feedback control system is deemed as asymptotically stable, provided that the Popov inequality[10] satisfies that

$$\eta(t_1)=\int_0^{t_1}\tilde{\varphi}^T(t)\varpi(t)\epsilon(t)\,\mathrm{d}t\geq -d^2 \tag{32}$$

which can readily be examined below:

$$\eta(t_1)=\int_0^{t_1}\tilde{\varphi}^T(t)\dot{\tilde{\varphi}}(t)\,\mathrm{d}t=\frac{1}{2\gamma}\left[\tilde{\varphi}^T(t_1)\tilde{\varphi}(t_1)-\tilde{\varphi}^T(0)\tilde{\varphi}(0)\right]$$
$$\geq -\frac{1}{2\gamma}\tilde{\varphi}^T(0)\tilde{\varphi}(0) \tag{33}$$

which guarantees the asymptotic stability for the proposed control system. Note that the inequality relationship in Eq. (33) requires that the adaptation gain γ be positive.

The study described in this section can now be used to bring about an adaptive feedforward control design for the active band-drive suspension system. Two kinds of numerical simulations have been implemented and are discussed in Sec. V.

V. Simulation Results

The model parameters of an active band-drive suspension system with two test articles for simulations are summarized in Table 1, including the control parameters used in this paper. A noncontrol suspension is simulated for comparison with the adaptive feedforward control system. Two kinds of initial excitations have been employed for simulations: 1) initial displacement and 2) initial velocity, imposed on the suspended masses. A 10-s suspension task is then assigned to the band-drive suspension system undergoing the structural testing.

In the first simulation, −0.2 and 0.2 in. of initial displacements are specified to masses m_1 and m_2, respectively, but with no initial velocity. Figures 5a–5d show the numerical results of this simulation. Figures 5a and 5b show the angle of the disk and the displacement of the mass m_2, respectively. The results associated with the adaptive feedforward control are indicated by a solid line; those with no control are indicated by a dashed line. Note that the dotted curve represents a desired trajectory from the reference model. The disk angle and the mass displacement in the solid line overlap those produced by the reference model after 5 s, whereas the dashed lines deviate from those attributable to the inertial loading. Under adaptive feedforward control, the time histories in Figs. 5a and 5b represent pure oscillatory motions about their equilibrium positions, corresponding to the anticipated vibrational characteristics of masses m_1 and m_2 in the zero gravity of space. Figure 5c demonstrates the transient responses of the error signals $\varepsilon(t)$ and $\dot{\varepsilon}(t)$, respectively, for the adaptive feedforward control. These error signals are considerably suppressed within 3 s by using the adaptive feedforward control. The responses of two voltage inputs corresponding to the

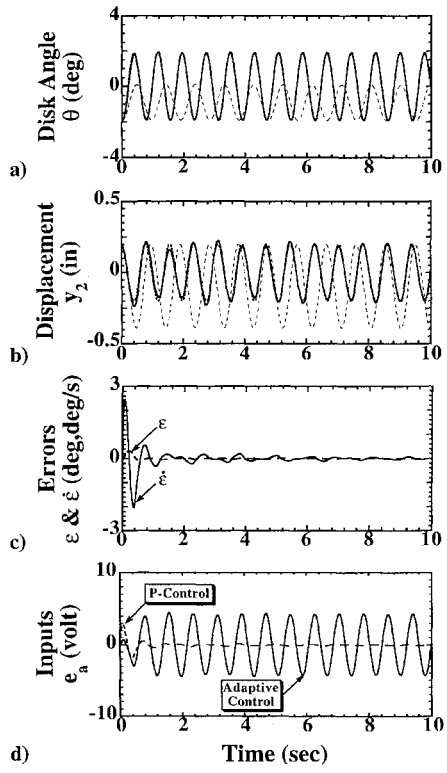

Fig. 5 Simulation results of a lumped-parameter model subject to the excitation of initial displacement.

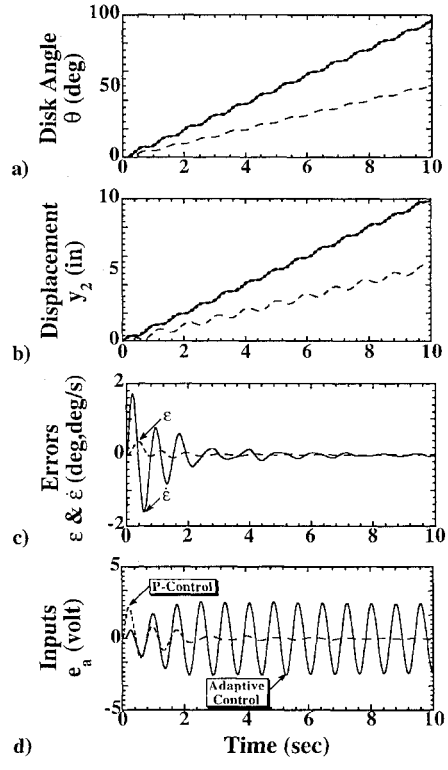

Fig. 6 Simulation results of a lumped-parameter model subject to the excitation of initial velocity.

feedback control and the adaptive feedforward control are shown in Fig. 5d. Note that the voltage history of feedback control rapidly converges as fast as the error signals in Fig. 5c, whereas that of adaptive feedforward control, in response to the oscillatory signals from the reference model, wobbles within the range of 5.0 V.

The second simulation deals with the dynamic responses subjected to an initial velocity specification. An initial velocity of 2.0 in./s acts on mass m_2 to excite the whole system to move as if under

an impulse. Figures 6a and 6b show the dynamic histories of the disk angle θ and the mass displacement y_2. The control results overlap those from the reference model, whereas the noncontrol results drift away from the desired trajectories. Figure 6a shows an oscillatory motion of the disk but with an average angular velocity of 9.5 deg/s superimposed upon that oscillation. Figure 6b shows that the entire test object is dropping at a constant velocity, while masses m_1 and m_2 are oscillating during this downward motion. This indicates that with the use of this band-drive suspension system the impulsive response indeed corresponds to that in a zero-gravity condition. Figure 6c illustrates the amplitudes of error signals under the adaptive feedforward control, and Fig. 6d shows the time histories of the two control inputs.

The motion of the rotating disk in the band-drive suspension system, under the presence of inertial loading, is shown to match a desired trajectory when the adaptive feedforward control law is invoked. The tracking error appearing in adaptation has been effectively suppressed through an adaptive feedforward controller. The simulation results in Figs. 5 and 6 thus validate the applicability of the proposed control design for the band-drive suspension system.

VI. Conclusions

A band-drive suspension system is integrated with a dc motor in conjunction with an adaptive feedforward controller for application to ground-based structural testing. The problem of adaptive suspension control of the nonlinear effects of the inertial loads on this suspension device are proposed and analyzed under the adaptive feedforward control. The results demonstrate the significant changes in the dynamic behavior of the suspension system resulting from inertial loading. An investigation of an adaptive feedforward control approach was conducted for the band-drive suspension system. The basic idea of the proposed control strategy is to adjust the adaptation parameters using the gradient method to minimize the tracking errors so that the closed-loop performance closely matches performances embodied in the reference model, while attempting to compensate for the inertial loads for the suspension system. To analyze the stability of the control algorithm, we used a lumped-parameter model formulated to work for the adaptive system, in which the adaptation law is proved to be asymptotically stable under the hyperstability theory.

Numerical simulations of the proposed control strategy are suitable for the band-drive suspension system to be used actively against the inertial loads in ground-based structural testing. The open-loop simulation results indicate that the noncircular disk deviates from the desired trajectory while losing the suspension capability. On the other hand, the control simulation results demonstrate that the adaptive feedforward controller is effective in recovering the deviated disk during suspension.

The present study shows that this control synthesis can be an attractive alternative to other existing control designs for the band-drive suspension system. However, much work needs to be done before the proposed strategy can be evaluated on a real-board prototype. Such work includes robustness when subjected to the disturbances and parametric uncertainties and cost-effectiveness, among others.

Acknowledgment

The authors wish to acknowledge the support of this investigation through Taiwan National Science Council Grant 84-2212-E-194-013.

References

[1]Chew, M.-S., Juang, J.-N., and Yang, L.-F., "Suspension Device for Low Frequency Structures," U.S. Patent No. 5,207,110, May 1993.

[2]Kienholz, D. A., "A Pneumatic/Electric Suspension Device for Very Low Frequency Dynamic Testing," AIAA Paper 89-2590, Nov. 1989.

[3]Woodard, S. E., and Housner, J. M., "Nonlinear Behavior of a Passive Zero-Spring-Rate Suspension System," *Journal of Guidance, Control, and Dynamics*, Vol. 14, No. 1, 1991, pp. 84–89.

[4]Yang, L.-F., Chew, M.-S., and Juang, J.-N., "Band-Drive Suspension Mechanism Design for Ground-Based Testing of Flexible Space Structures," *Journal of Mechanical Design*, Vol. 117, March 1995, pp. 134–142.

[5]Åström, K. J., and Wittenmark, B., *Adaptive Control*, 2nd ed., Addison–Wesley, Reading, MA, 1995, pp. 185–199.

[6]Tomizuka, M., Hu, J.-S., Chiu, T.-C., and Kamano, T., "Synchronization of Two Motion Control Axes Under Adaptive Feedforward Control," *Journal of Dynamic Systems, Measurement and Control*, Vol. 114, June 1992, pp. 196–203.

[7]Yang, L.-F., and Chang, W.-H., "Synchronization of Twin-Gyro Precession Under Cross-Coupled Adaptive Feedforward Control," *Proceedings of the AIAA/ASME/ASCE/AHS 36th Structures, Structural Dynamics, and Materials Conference* (New Orleans, LA), AIAA, Washington, DC, 1995, pp. 903–912.

[8]Yang, L.-F., and Tsao, J.-G., "Adaptive Synchronization Control Design for High-Speed Magnetic Bearings," *Proceedings of ASME 15th Biennial Conference on Mechanical Vibration and Noise* (Boston, MA), American Society of Mechanical Engineers, New York, 1995, pp. 1093–1102.

[9]Park, K. C., Chiou, J.-C., and Downer, J. D., "Explicit-Implicit Staggered Procedure for Multibody Dynamics Analysis," *Journal of Guidance, Control, and Dynamics*, Vol. 13, No. 3, 1990, pp. 562–570.

[10]Popov, V. M., *Hyperstability of Control Systems*, Springer–Verlag, Berlin, 1973, pp. 118–235.